

---

# SegEarth-R1: Geospatial Pixel Reasoning via Large Language Model

---

Kaiyu Li<sup>1,\*</sup>, Zepeng Xin<sup>1,\*</sup>, Li Pang<sup>1</sup>, Chao Pang<sup>2</sup>, Yupeng Deng<sup>3</sup>  
Jing Yao<sup>3</sup>, Guisong Xia<sup>2</sup>, Deyu Meng<sup>1</sup>, Zhi Wang<sup>1</sup>, Xiangyong Cao<sup>1,†</sup>  
<sup>1</sup>Xi'an Jiaotong University   <sup>2</sup>Wuhan University   <sup>3</sup>Chinese Academy of Sciences

## Abstract

Remote sensing has become critical for understanding environmental dynamics, urban planning, and disaster management. However, traditional remote sensing workflows often rely on explicit segmentation or detection methods, which struggle to handle complex, implicit queries that require reasoning over spatial context, domain knowledge, and implicit user intent. Motivated by this, we introduce a new task, *i.e.*, geospatial pixel reasoning, which allows implicit querying and reasoning and generates the mask of the target region. To advance this task, we construct and release the first large-scale benchmark dataset called EarthReason, which comprises 5,434 manually annotated image masks with over 30,000 implicit question-answer pairs. Moreover, we propose SegEarth-R1, a simple yet effective language-guided segmentation baseline that integrates a hierarchical visual encoder, a large language model (LLM) for instruction parsing, and a tailored mask generator for spatial correlation. The design of SegEarth-R1 incorporates domain-specific adaptations, including aggressive visual token compression to handle ultra-high-resolution remote sensing images, a description projection module to fuse language and multi-scale features, and a streamlined mask prediction pipeline that directly queries description embeddings. Extensive experiments demonstrate that SegEarth-R1 achieves state-of-the-art performance on both reasoning and referring segmentation tasks, significantly outperforming traditional and LLM-based segmentation methods. Our data and code will be released at <https://github.com/earth-insights/SegEarth-R1>.

## 1 Introduction

Earth observation through remote sensing has emerged as a cornerstone of modern geospatial analysis, enabling unprecedented insights into environmental dynamics, urban planning, and disaster management [56, 45]. Satellite and aerial images provide a unique vantage point for monitoring planetary-scale phenomena, ranging from deforestation patterns to coastal erosion. However, converting this raw pixel data into actionable insights requires more than traditional computer vision techniques; it demands models capable of reasoning about spatial context, domain knowledge, and implicit user intent. Conventional remote sensing workflows predominantly rely on explicit tasks, *e.g.*, semantic segmentation and referring segmentation [44, 8, 85], which operate within fixed taxonomies and require precise user instructions. While effective for well-defined scenarios, these approaches struggle to accommodate complex, implicit queries—for example, identifying regions at elevated risk of landslides based on slope, vegetation cover, and proximity to infrastructure. Such tasks limit implicit reasoning over heterogeneous spatial patterns, object relationships, and environmental metadata, exceeding the capabilities of standard segmentation or detection pipelines.

Motivated by this, we introduce a new task, *i.e.*, geospatial pixel reasoning, which allows implicit querying and reasoning and generates the mask of the target region. To enable research in this task,

---

\*Equal contribution

†Corresponding author: caoxiangyong@mail.xjtu.edu.cn

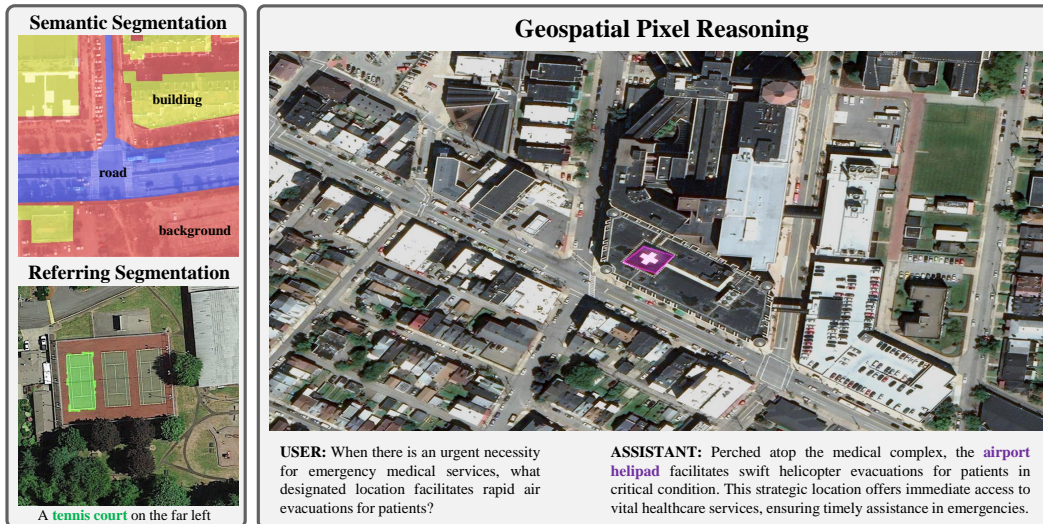


Figure 1: Comparison of semantic segmentation, referring segmentation and geospatial pixel inference. (left) Samples from the LoveDA [67] and RRSIS-D [40] datasets. (right) Samples from the EarthReason dataset. Previous tasks are limited by fixed taxonomies and explicit instructions, while geospatial pixel reasoning supports complex implicit instructions and requires the reasoning capability of the model.

we build and release the first large-scale benchmark dataset, called EarthReason, which contains 5,434 manually annotated remote sensing image-mask pairs drawn from diverse classification sources, covering 28 scene categories at spatial resolutions ranging from 0.5m to 153m. Each image is paired with multiple implicit reasoning questions that require the model to infer target masks based on contextual and domain-specific knowledge, rather than explicit object names. In addition, by incorporating empty target cases and varying spatial scales, EarthReason pushes models to generalize across complex real-world remote sensing scenarios.

Recent progress in multimodal large language models (MLLMs) has demonstrated impressive performance in natural image domains, where models like LISA [26] and PixelLM [55] leverage large language models (LLMs) [62, 7, 79] to interpret rich textual prompts and generate pixel-level outputs. These frameworks excel at tasks such as reasoning segmentation [26], where the target mask is not directly specified but must be inferred from nuanced language cues. Unfortunately, directly transferring these methods to geospatial pixel reasoning is non-trivial since remote sensing images present extreme scale variation, densely packed small-scale objects and ultra-high resolution that violate assumptions of natural images. Moreover, different from natural images, remote sensing queries often require spatial correlations. For instance, identifying “informal settlements” relies on detecting roof material irregularities, road network fragmentation, and spatial adjacency to legal land-use zones.

To address these challenges, we present SegEarth-R1, a simple yet effective language-guided segmentation model that integrates a hierarchical visual encoder, an LLM for instruction parsing, and a tailored mask generator designed for spatial correlation. Further, some components are also designed to adapt to the characteristics of remote sensing images. Specifically, we propose the aggressive visual token compression to handle ultra-high-resolution images, a description projection module to fuse language and multi-scale features, and a streamlined mask prediction pipeline that directly queries description embeddings. Despite its architectural simplicity, SegEarth-R1 achieves advanced performance on EarthReason and referring segmentation datasets, significantly outperforming both traditional and LLM-based segmentation methods.

In summary, our contributions are as follows:

- We introduce the geospatial pixel reasoning task, which requires models to infer segmentation masks from implicit natural language queries by reasoning over spatial context and domain knowledge.
- We build and release the first large-scale benchmark with 5,434 image-mask pairs, 28 categories, and over 30,000 implicit question-answer pairs, fostering research in geospatial pixel reasoning.

- We propose an LLM-based segmentation model, SegEarth-R1, which incorporates new segmentation capabilities in remote sensing, containing several domain-specific designs.
- Extensive experiments show that SegEarth-R1 achieves state-of-the-art performance on reasoning and referring segmentation tasks, compared to traditional methods and other LLM-based methods.

## 2 Related Work

### 2.1 Referring Segmentation

Referring segmentation aims to segment targets in an image based on natural language descriptions, requiring precise alignment between linguistic expressions and visual content. Early approaches adopted CNN-RNN/LSTM frameworks [18, 36, 32, 47, 60, 21] to extract visual features and encode textual queries, respectively. However, these methods struggled with complex expressions due to limited local receptive fields and insufficient cross-modal interaction [24]. To address these limitations, attention mechanisms [63] emerged as a pivotal technique [10, 81, 72, 19, 77, 49, 74, 58]. VLT [10] dynamically generates adaptive query vectors based on image-text interactions, enabling precise localization through cross-modal attention. LAVT [81] further advances this paradigm by integrating hierarchical visual-linguistic fusion within a Swin Transformer [43] backbone, where pixel-word attention refines multiscale features to achieve fine-grained semantic alignment. In remote sensing, specifying segmentation for certain instances can improve interpretation efficiency and user interactivity. Recently, Yuan *et al.* [85] introduced referring segmentation into satellite images for the first time. Subsequently, following the LAVT [81] architecture, RMSIN [40] also incorporated adaptive rotated convolutions to address scale and orientation variations. FIANet [28] and CroBIM [12] introduced elaborate cross-modal interactions for feature alignment. RSSep [17] reformulated referring segmentation as a sequence-to-sequence task, predicting polygonal boundaries to handle scale variations and blurred edges [38]. However, existing methods effectively follow explicit instructions for target segmentation but lack implicit intent reasoning. In this paper, the proposed geospatial pixel reasoning task advances beyond referring segmentation by employing LLMs’ reasoning capabilities to interpret subtle instructions and accurately segment desired targets.

### 2.2 LLM-based Segmentation

Recent advances in LLMs have significantly expanded their capabilities to integrate pixel-level segmentation with language reasoning [76, 68, 73, 2, 61, 88, 84, 16]. For instance, Florence-2 [76] unified text, detection, and segmentation through a sequence-to-sequence framework with task instructions. To address the complexity of real-world segmentation scenarios, some works focus on architectural specialization and instruction-aware adaptation. LISA [26, 80] established the paradigm by introducing a [SEG] token to connect LLMs with segmentation decoders like SAM [25], enabling language-guided mask prediction. Subsequent studies enhanced this paradigm: GSVA [75] introduced shared-weight [SEG] tokens and [REJ] tokens for multi-target and empty-target handling [35, 55, 90], while GLaMM [53] achieved pixel-grounded conversational capabilities through holistic segmentation [94]. Parallel efforts focused on architectural unification - PSALM [92] established a flexible input schema for multi-task segmentation, and OMG-LLaVA [89] combined universal segmentation backbones with LLMs for pixel-level reasoning. Video understanding extensions emerged through VISA [78] and InstructSeg [71], which integrated temporal reasoning. Notably, Text4Seg [27] redefined segmentation as a text generation problem using semantic descriptors, eliminating the need for an additional decoder. In remote sensing, benefiting from the above paradigms [26, 27], some unified models such as RSUniVLM [42], GeoGround [95] and GeoPix [50] are equipped with segmentation capabilities. Although based on LLM, these models focus only on explicit text-guided segmentation. Further, GeoPixel [57] introduced grounded conversation generation [53] to remote sensing, but it still does not provide reasoning capability. Our SegEarth-R1 also follows the LLM-based segmentation paradigm, but is different from previous methods. Specifically, SegEarth-R1 is the first work to support reasoning about the target region from implicit queries, and its components are specifically designed for the challenges in remote sensing.

Table 1: Comparison between EarthReason and other related datasets. The gray rendering denotes the natural image dataset. “Seg”, “Det”, “VG”, “Cls” denote segmentation, detection, visual grounding and classification datasets, respectively.

Dataset	Mask Label	Reasoning Query	Spatial resolution	Image Size	Image Num	Image Source	Class Num
ReasonSeg [26]	✓	✓	-	-	1,218	OpenImages (Seg) & ScanNetv2 (Seg)	-
LLM-Seg40K [65]	✓	✓	-	-	14,000	LVIS (Seg) & EgoObjects (Seg)	-
EarthVQA [66]	✗	✓	0.3m	1024 <sup>2</sup>	6,000	LoveDA (Seg)	14
RegSegRS [85]	✓	✗	0.5m-30m	800 <sup>2</sup>	4,420	SkyScapes (Seg)	14
RRSIS-D [40]	✓	✗	0.13m	512 <sup>2</sup>	17,402	RSVGD (VG) & DIOR (OD)	20
RISBench [12]	✓	✗	0.1m-30m	512 <sup>2</sup>	52,472	DOTAv2(OD) & DIOR (OD)	26
EarthReason	✓	✓	0.5m-153m	123 <sup>2</sup> -7617 <sup>2</sup>	5,434	AID (Cls) & fMoW (Cls)	28

### 3 Benchmark Geospatial Pixel Reasoning Dataset—EarthReason

#### 3.1 Comparison with Related Dataset

We analyze three types of tasks and datasets related to geospatial pixel reasoning, *i.e.*, natural image reasoning segmentation, remote sensing visual question answering (VQA), and remote sensing referring segmentation, as shown in Table 1. RefSegRS [85] and RRSIS-D [40] provide early benchmarks with image-text-mask triplets. RISBench [12], the largest RRSIS dataset to date, introduced 52,472 triplets with oriented bounding boxes and pixel-level masks generated via a semi-automatic pipeline. These datasets address the limitations of earlier text-focused datasets (*e.g.*, RSICD [46], EarthVQA [66], *etc.*) and enable comprehensive evaluation of multimodal models. Compared to the previous referring segmentation datasets, our EarthReason datasets has the following features: **(1)** The mask labels in EarthReason are not explicitly specified by the query, but require further reasoning to determine the target, which challenges the model’s reasoning ability. **(2)** EarthReason uses a more raw data source. The previous related datasets directly transform existing segmentation datasets [1, 67] or SAM-processed detection datasets [86, 31, 11], while our EarthReason uses images from classification datasets [44, 8] and we manually annotate them. This allows EarthReason to provide more data gain when it comes to co-training of unified segmentation tasks. **(3)** EarthReason has more diverse spatial resolutions and image sizes, which are conducive to solving the object scale spanning problem inherent in remote sensing images [56]. Compared to the first natural image reasoning segmentation dataset, ReasonSeg, EarthReason contains  $4.46\times$  more data than it. Therefore, we believe that EarthReason, as the first geospatial pixel reasoning dataset in the remote sensing area, is capable of performing initial explorations of this task.

#### 3.2 Dataset Generation Pipeline

Our benchmark dataset EarthReason is generated according to the following three steps, *i.e.*, image collection, question-answer pair generation, and object mask labeling.

**Image Collection.** As mentioned above, to avoid potential data leakage in the future construction of unified segmentation models for remote sensing, we collect images from existing classification data. Although this increases the annotation cost, it also motivates more diverse scenes. Specifically, we first select the 28 categories that are more suitable for reasoning in the Million-AID [44] dataset, and sample about 200 images for each category. Then, we find that the actual geographic range contained in Million-AID’s images is limited. Thus, we also collect 800 images in the fMoW [8] dataset to enhance the model’s reasoning ability in complex scenes. Further, to alleviate the factitious illusion issue [51], we add an extra 200 empty target images (*i.e.*, the implied target is not in the image). Finally, some low-quality images are eliminated, and we obtain a total of 5,434 images.

**Question-Answer Pair Generation.** We use GPT-4o<sup>1</sup> to construct question-answer pairs, and given its excellent visual comprehension, we take the remote sensing image and the corresponding scene category (provided by Million-AID and fMoW) as part of the prompt to generate questions and answers that are closely related to the image. An example of such a prompt is illustrated in Appendix A.1. In addition, following [26], to make the questions and answers diverse, we adapt GPT-3.5 to rephrase the instructional questions and answers, as shown in Appendix Figure 7.

<sup>1</sup><https://platform.openai.com/docs/models/gpt-4o>

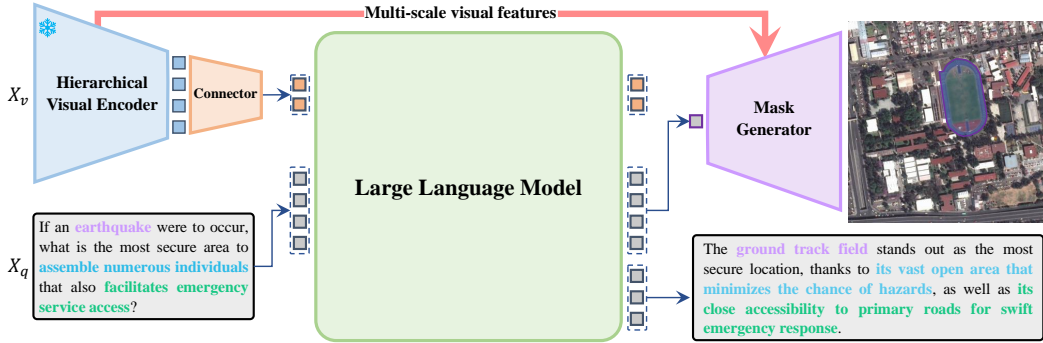


Figure 2: Overview of the proposed SegEarth-R1 architecture. Given an image  $X_v$  and a text description  $X_q$ , a hierarchical visual encoder and a proposed connector are used to extract and compress visual tokens. Then, the visual tokens  $\square$  and description embeddings  $\square$  are fed into an LLM for instruction interpretation and semantic correlation. Finally, description embeddings are directly mapped to the query vector and used for spatial correlation and segmentation mask generation.

**Object Mask Labeling.** Different from previous referring and reasoning segmentation datasets (which use off-the-shelf masks or bounding boxes), we annotate images from scratch. Specifically, we employ multiple experts in remote sensing and vision, assign each expert a few hundred images to annotate, and cross-validate the annotations after they are completed. For simple targets (*e.g.*, lake), SAM-H [25] is used to assist in annotation; for complex targets (*e.g.*, wind turbine), each point of the polygon is finely marked. A description of mask quality is provided in Appendix A.1.

**Dataset Statistics.** The EarthReason dataset is partitioned into training, validation, and testing sets, comprising 2,371, 1,135, and 1,928 images, respectively. In the training set, each image is annotated with an average of six questions and three corresponding answers. The average question length is 20.86 words, while the average answer length is 26.76 words. To assess the model’s generalization capability, several semantic categories are deliberately reserved for the validation and test sets, ensuring they remain unseen during training. Additional dataset details are provided in the Appendix A.2.

## 4 Baseline Geospatial Pixel Reasoning Method—SegEarth-R1

Compared with natural images, remote sensing images exhibit distinctive characteristics that demand specialized architectural designs for pixel-wise geospatial reasoning. In this work, we propose SegEarth-R1, a simple yet powerful baseline for geospatial pixel reasoning that effectively harnesses LLM capabilities while incorporating domain-specific adaptations. As illustrated in Figure 2, our architecture comprises three core parts: A visual encoder for image feature extraction, an LLM for instruction interpretation and semantic correlation, and a mask generator for spatial correlation and mask prediction. Each part incorporates critical design considerations to address the unique challenges of remote sensing images.

### 4.1 Hierarchical Visual Encoder

Satellite and aerial targets present two critical challenges: (1) extreme scale variations ranging from sub-meter objects to kilometer-scale geographical formations [56], and (2) densely distributed small objects requiring high-resolution analysis [30]. Conventional ViT-based encoders adopted in MLLMs [26, 80, 25, 75] (*e.g.*, image encoder in CLIP [52] and SAM [25, 54]) prove suboptimal due to their fixed-scale feature extraction and information compression through aggressive patch merging. To alleviate these limitations, following [92], SegEarth-R1 employs a Swin Transformer [43] backbone enhanced with progressive feature hierarchy construction. This architecture generates multi-scale feature maps  $v_h, h \in [1, 4]$  at  $1/4, 1/8, 1/16, 1/32$  of the original resolution through controlled downsampling operations, preserving high-resolution details for small objects while capturing contextual semantics at deeper layers.

## 4.2 Large Language Model and Input Schema

SegEarth-R1 adopts the MLLM paradigm [37, 29] by jointly embedding visual tokens and textual instructions into a unified LLM input space for multimodal reasoning. Unlike natural images, remote sensing data exhibits ultra-high-resolution coverage [23, 64], posing computational challenges when processed through billion-level LLMs. Therefore, we expect to compress the visual token to alleviate the computational cost and make only simple semantic correlations in LLM.

### 4.2.1 Visual Token

**Redundancy Analysis.** Image redundancy quantifies the proportion of compressible, non-informative data within an image. To investigate the feasibility of aggressive visual token compression for remote sensing images, we conduct a redundancy analysis from dual perspectives: pixel-level statistical redundancy and spatial structural redundancy.

- According to information theory [59], entropy measures the average uncertainty or information content of an image, while the maximum entropy corresponds to the idealized scenario where pixel values are uniformly distributed (*i.e.*, no redundancy). Thus, from the entropy perspective, the image redundancy can be defined as [14]:

$$R_e = 1 - \frac{-\sum_{l=0}^{L-1} p(l) \log_2 p(l)}{\log_2 L}, \quad (1)$$

where  $L$  denotes the number of distinct intensity levels (*e.g.*,  $L = 256$  for an 8-bit grayscale image), and  $p(l)$  denotes the probability mass function of the pixel intensity value  $l$ .

- Beyond pixel-level statistical redundancy, structural self-similarity reflects spatial redundancy caused by repetitive patterns (*e.g.*, textures, geometric features). To quantify this, we leverage the Structural Similarity Index Matrix (SSIM) [70] to measure inter-patch similarity. For an image partitioned into  $N$  patches, the SSIM matrix  $\mathbf{M} \in \mathbb{R}^{N \times N}$  is defined as:

$$\mathbf{M}(i, j) = \frac{(2\mu_i\mu_j + C_1)(2\sigma_{ij} + C_2)}{(\mu_i^2 + \mu_j^2 + C_1)(\sigma_i^2 + \sigma_j^2 + C_2)}, \quad \forall i, j \in 1, \dots, N \quad (2)$$

where  $\mu_i, \sigma_i$  denote the mean and variance of the  $i$ -th patch,  $\sigma_{ij}$  is the covariance between patches  $i$  and  $j$ , and  $C_1, C_2$  are stability constants. Then, the structural self-similarity redundancy  $R_s$  is derived by averaging off-diagonal elements of  $\mathbf{M}$ :

$$R_s = \frac{1}{N(N-1)} \sum_{i \neq j} \mathbf{M}(i, j). \quad (3)$$

We evaluate six benchmark datasets spanning natural images (COCO [3], ADE20K [93], PASCAL [13]) and remote sensing images (LoveDA [67], DeepGlobe [9], xBD [15]) for redundancy analysis. As shown in Figure 3, our analysis reveals two critical findings: 1) Remote sensing images demonstrate 1.9~3.3× higher entropic redundancy than natural images, indicating greater pixel-level compressibility. 2) The average self-similarity for remote sensing data exceeds natural images by 42.6%, confirming the higher prevalence of repetitive textures and geometric patterns. This insight justifies aggressive token compression for semantic-level comprehension in remote sensing images.

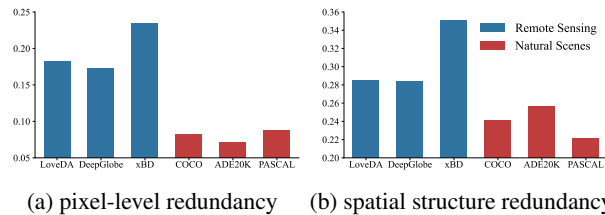


Figure 3: Redundancy analysis of remote sensing datasets and natural images, and the former exhibits higher redundancy.

**Token Compression Connector.** In modern MLLM, connectors such as Q-Former [29] and MLP [37] are designed to transform visual tokens into a multi-modal space. However, some works [4, 82] point out that Q-Former may lead to loss of vision information and is difficult to train. Therefore, in SegEarth-R1, we follow the MLP connector fashion in LLaVA [37] and use a simple but effective connector, *i.e.*, stacked convolutional blocks and Layer Normalization (LN). Here, convolutional

blocks are used for spatial down-sampling to compress the size of the feature map, and LN is used to stabilize cross-modal training. Specifically, our connector can be formulated as:

$$v_{out} = (Conv \circ LN)^d(v_4), \quad (4)$$

where  $\circ$  denotes the function composition operator, and  $d$  denotes the number of stacked layers.

### 4.2.2 Text Instruction

Although the instructions involved in geospatial pixel reasoning are implicit and contain more words than referring segmentation, they still maintain the same data format. Therefore, it is easy to convert them into question-answer pairs using a template like “**USER:** This is an image <IMAGE>, please doing geospatial pixel reasoning according to the following instruction: <DESCRIPTION>. **ASSISTANT:** <ANSWER>”. For referring segmentation task, the task name in the instruction is changed to “referring segmentation”.

### 4.3 Mask Generation with Spatial Correlation

Some recent LLM-based segmentation models [92, 71] use Mask2Former [5] paradigm as mask generator. They use  $T$  learnable mask tokens (typically  $T=100$ ) as queries in the transformer decoder to generate  $T$  candidate masks with corresponding scores, which are then assigned to the description embeddings<sup>2</sup> by bipartite matching. Unlike the reasoning segmentation of natural images, which is more inclined to make inferences based on the attributes of the object itself. In geospatial pixel reasoning, the model must understand and extrapolate more based on the spatial layout and inter-object correlations within the image (e.g., identifying earthquake evacuation zones in Figure 2, which requires analyzing topological relationships between roads and buildings). In addition, we posit that the mask query mechanism [6, 5] is inflexible and redundant in language-guided segmentation, and we only need to generate variable numbers of masks based on the instruction. Motivated by the above, we propose to directly use description embedding as the query for the mask generator and explicitly associate it with the image spatial features.

The length of description embeddings varies according to the user’s instruction, whereas in our geospatial pixel reasoning or referring segmentation setting, the segmentation result can be represented by a single binary mask. Therefore, we introduce a description projection module ( $D$ -Projector), which converts the whole description into a single vector as shown in Figure 4. Specifically, the description embeddings are averaged into a global vector, which is then interacted with the flattened multi-scale visual features via a cross-attention operation, and a skip-connection and linear layer maps it into the query vector. Following this, the query vector is fed into the Transformer decoder of Mask2Former, which is composed of stacked masked attention, self-attention and FFN. Notably, since the mask query mechanism has been removed, the number of generated masks is the same as the number of queries, and therefore, score prediction and bipartite matching are also not required. Finally, the predicted mask is supervised with a linear combination of focal loss [34] and dice loss [48].

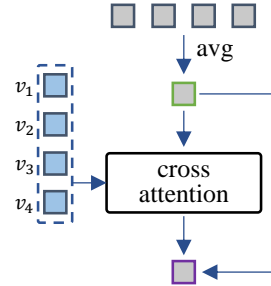


Figure 4:  $D$ -Projector.

## 5 Experiments

### 5.1 Settings

**Datasets and Tasks.** In addition to the geospatial pixel reasoning on EarthReason, we assess the basic geolocation capability with the explicit short query of our model. We employed two benchmark referring image segmentation datasets: RefSegRS [85] and RRSIS-D [40]. These datasets contain 14 and 20 semantic categories, respectively, with textual descriptions primarily focusing on direct visual attributes such as orientation, color, and size. All models are trained on their own training set and evaluated on their validation and testing sets.

**Evaluation metrics.** Following [26], we adopt two evaluation metrics: **gIoU** (per-image IoU average) and **cIoU** (cumulative intersection over union). The latter is preferred because of its stability.

<sup>2</sup>embeddings of <DESCRIPTION> in text instruction.

**Network Architecture.** Unless otherwise specified, SegEarth-R1 use phi-1.5 (1.3B) [33] as the LLM, and adopt the Swin-B as the visual encoder. The token compression connector is configured with a layer number  $d = 2$ . The mask generator follows the Mask2Former architecture, but removes mask tokens as mentioned above.

**Implementation details.** During training, we use bf16 precision and freeze the visual encoder. The LLM is initialized from Phi-1.5, while both the Swin-B encoder and the mask generator are initialized with pretrained weights from Mask2Former. All images are resized to  $1024 \times 1024$ , maintaining the original aspect ratio by padding the shorter side. We adopt the AdamW optimizer with an initial learning rate of  $1 \times 10^{-4}$ , cosine learning rate schedule, and no weight decay. A uniform batch size of 16 is used across datasets, with training steps set to 7,610 (RRSIS-D), 5,400 (RefSegRS), and 2,220 (EarthReason). All experiments are conducted on two NVIDIA A100 80GB GPUs.

## 5.2 Geospatial Pixel Reasoning Results

Table 2: Geospatial pixel reasoning results among SegEarth-R1 (ours) and previous related works.

Method	Visual Encoder	LLM Type	cloU		gIoU	
			Val	Test	Val	Test
LISA [26]	CLIP-L	Vicuna-7B [7]	57.39	59.10	61.04	60.88
PixelLM [55]	CLIP-L	Vicuna-7B [7]	57.79	59.22	57.94	60.01
PSALM [92]	Swin-B	phi-1.5 (1.3B) [33]	62.03	64.61	66.61	68.30
<i>SegEarth-R1</i>	Swin-B	phi-1.5 (1.3B) [33]	<b>64.13</b>	<b>68.25</b>	<b>68.60</b>	<b>70.75</b>

We conduct a comparative evaluation of SOTA LLM-based methods and SegEarth-R1 on the EarthReason dataset. As shown in Table 2, all models are trained solely on the training split of EarthReason to ensure a fair comparison.

LISA and PixelLM demonstrate comparable performance; however, despite leveraging larger LLM or MLLM, the quality of their predicted segmentation masks remains suboptimal. This can be primarily attributed to their reliance on CLIP as the visual encoder, which tends to diminish the representation of small-scale geospatial targets. As one of the baselines of SegEarth-R1, PSALM achieves notable improvements over LISA and PixelLM. Nevertheless, PSALM does not adequately incorporate LLM-based segmentation and the Mask2Former paradigm, and lacks considerations for overhead images. SegEarth-R1 achieves the best results on both metrics surpassing PSALM by 3.64% and 2.45% on the test set. Importantly, SegEarth-R1 uses fewer visual tokens in LLM and reduces the number of queries in the mask generator, thus providing a lower inference cost.

## 5.3 Referring Segmentation Results

SegEarth-R1 also supports basic explicit language-guided segmentation. As shown in Table 3, we compare its performance with existing SOTA traditional methods (not based on LLM) as well as recent LLM-based methods. Notably, prior to SegEarth-R1, LLM-based methods consistently underperformed in comparison to traditional methods on the referring segmentation task. For instance, the advanced GeoGround [95] lags behind RMSIN [40] by 3.7% in terms of gIoU on the RRSIS-D dataset. In contrast, SegEarth-R1, as a universal LLM-based language-guided segmentation method, surpasses traditional methods on the referring segmentation task for the first time with a 2.2% improvement. This result highlights the enhanced generalization capability and practical potential of SegEarth-R1. On the RefSegRS dataset, the improvement of SegEarth-R1 is more significant than the previous method, with an 8.33% and 9.87% improvement over RMSIN on the validation and testing sets, respectively, as listed in Table 4.

Table 3: Referring segmentation results among SegEarth-R1 and previous related works on RRSIS-D dataset.

Method		P@0.5		cloU		gIoU	
		Val	Test	Val	Test	Val	Test
<b>Traditional method:</b>							
RRN [32]	CVPR'18	51.09	51.07	66.53	66.43	46.06	45.64
CSMC [83]	CVPR'19	55.68	55.32	69.39	69.39	48.85	48.54
LSCM [22]	ECCV'20	57.12	56.02	69.05	69.28	50.36	49.92
CMPC [21]	CVPR'20	57.93	55.83	69.22	69.39	50.41	49.24
BRINet [20]	CVPR'20	58.79	56.90	70.73	69.88	51.14	49.65
CMPC+ [39]	TPAMI'20	59.19	57.65	70.14	68.64	51.41	50.24
LGCE [85]	TGRS'24	68.10	67.65	76.68	76.34	60.16	59.37
RIS-DMMI [19]	CVPR'23	70.40	68.74	77.01	76.20	60.72	60.12
LAVT [81]	CVPR'22	69.54	69.52	77.59	77.19	61.46	61.04
RMSIN [40]	CVPR'24	74.66	74.26	78.27	77.79	65.10	64.20
<b>LLM-based method:</b>							
LISA [26]	CVPR'24	27.07	24.51	-	-	27.84	26.78
PixelLM [55]	CVPR'24	33.46	28.81	-	-	33.89	31.65
NEXT-Chat [87]	arXiv'23	28.97	26.37	-	-	26.98	24.98
GeoGround [95]	arXiv'25	68.69	67.50	-	-	61.10	60.50
<i>SegEarth-R1</i>		<b>78.62</b>	<b>76.96</b>	<b>78.92</b>	<b>78.01</b>	<b>67.56</b>	<b>66.40</b>

Table 4: Referring segmentation results among SegEarth-R1 and previous related works on RefSegRS dataset.

Method		P@0.5		P@0.6		P@0.7		P@0.8		P@0.9		cloU		gIoU	
		Val	Test												
BRINet [20]	CVPR'20	36.86	20.72	35.53	14.26	19.93	9.87	10.66	2.98	2.84	1.14	61.59	58.22	38.73	31.51
LSCM [22]	ECCV'20	56.82	31.54	41.24	20.41	21.85	9.51	12.11	5.29	2.51	0.84	62.82	61.27	40.59	35.54
CMPC [21]	CVPR'20	46.09	32.36	26.45	14.14	12.76	6.55	7.42	1.76	1.39	0.22	63.55	55.39	42.08	40.63
CMSA [83]	CVPR'19	39.24	28.07	38.44	20.25	20.39	12.71	11.79	5.61	1.52	0.83	65.84	64.53	43.62	41.47
RRN [32]	CVPR'18	55.43	30.26	42.98	23.01	23.11	14.87	13.72	7.17	2.64	0.98	69.24	65.06	50.81	41.88
EVF-SAM [91]	Arxiv'24	57.77	35.17	37.59	22.34	16.24	9.36	4.87	2.86	1.86	0.39	59.61	55.51	46.98	36.64
CMPC+ [39]	TPAMI'21	56.84	49.19	37.59	28.31	20.42	15.31	10.67	8.12	2.78	0.55	70.62	66.53	47.13	43.65
CARIS [41]	ACMMM'23	68.45	45.40	47.10	27.19	25.52	15.08	14.62	8.87	3.71	1.98	75.79	69.74	54.30	42.66
CRIS [69]	CVPR'22	53.13	35.77	36.19	24.11	24.36	14.36	11.83	6.38	2.55	1.21	72.14	65.87	53.74	43.26
LAVT [81]	CVPR'22	80.97	51.84	58.70	30.27	31.09	17.34	15.55	9.52	4.64	2.09	78.50	71.86	61.53	47.40
RIS-DMMI [19]	CVPR'23	86.17	63.89	74.71	44.30	38.05	19.81	18.10	6.49	3.25	1.00	74.02	68.58	65.72	52.15
LGCE [85]	TGRS'24	90.72	73.75	86.31	61.14	71.93	39.46	32.95	16.02	10.21	5.45	83.56	76.81	72.51	59.96
RMSIN [40]	CVPR'24	93.97	79.20	89.33	65.99	74.25	42.98	29.70	16.51	7.89	3.25	82.41	75.72	73.84	62.58
SegEarth-R1		<b>95.82</b>	<b>86.30</b>	<b>93.27</b>	<b>79.53</b>	<b>88.86</b>	<b>69.57</b>	<b>78.19</b>	<b>48.87</b>	<b>22.04</b>	<b>10.73</b>	<b>85.01</b>	<b>79.00</b>	<b>82.17</b>	<b>72.45</b>

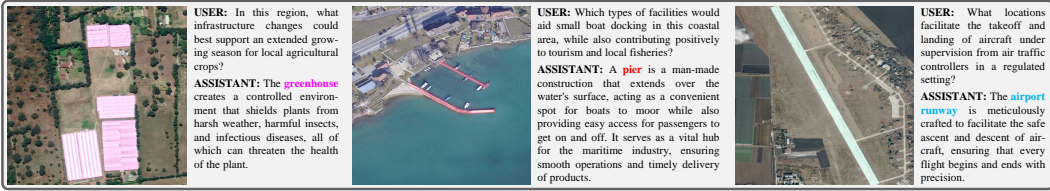


Figure 5: Qualitative Results of SegEarth-R1 on EarthReason. More results can be found in Appendix C.

#### 5.4 Ablation Study

Table 5: Ablation of SegEarth-R1 components on EarthReason: query description embedding (Query D.E.), description projector ( $D$ -Projector), token compression connector (T.C. Connector).

Query D.E.	$D$ -Projector	T.C. Connector	cloU		gIoU	
			Val	Test	Val	Test
$\times$	$\times$	$\times$	62.03	64.61	66.61	68.30
$\checkmark$	$\times$	$\times$	63.34	66.19	67.42	69.15
$\times$	$\checkmark$	$\times$	63.32	66.31	67.22	69.21
$\times$	$\times$	$\checkmark$	63.47	65.41	68.31	69.20
$\checkmark$	$\checkmark$	$\times$	64.12	66.71	<b>68.61</b>	69.61
$\checkmark$	$\checkmark$	$\checkmark$	<b>64.13</b>	<b>68.25</b>	68.60	<b>70.75</b>

**Components.** We conduct ablation studies on the EarthReason dataset to evaluate the effectiveness of the novel components involved in SegEarth-R1. As listed in Table 5, the first row shows the results of the PSALM baseline. Each proposed component contributes to performance enhancement, yielding improvements ranging from 0.85% to 0.9%. The T.C. Connector and Query D.E. not only enhances performance but also reduces computational overhead. Further, the proposed components can be well coupled, and when they are all activated, *i.e.*, complete SegEarth-R1, all metrics exhibit substantial gains over the baseline, confirming the effectiveness and compatibility of the proposed design. In fact, although these components are initially designed with remote sensing scenarios in mind, their underlying principles offer transferable insights applicable to general image understanding.

**LLM Type.** Given the limited scale of the dataset, we select some small LLM for comparison, as presented in Table 6. SegEarth-R1 demonstrates consistently high performance across different LLM, indicating the robustness and architectural stability of the overall framework. Notably, with Qwen2.5 (0.5B) [79], it still achieves competitive results, indicating its potential for edge deployment.

**Layer Number of T.C. Connector.** The layer number  $d$  controls the number of visual tokens fed into the LLM. As shown in Table 7, increasing token quantity does not improve performance. This observation aligns with our earlier analysis, suggesting that appropriate compression of visual tokens is beneficial for the global understanding of a remote sensing image. In SegEarth-R1, spatial correlations between the image and the instruction are primarily handled by the mask generator, while the LLM is only responsible for relatively semantic correlations. This division of labor allows for more efficient use of computational resources without compromising performance.

Table 6: Ablation of LLM type on RRSIS-D.

LLM Type	cloU		gIoU	
	Val	Test	Val	Test
phi-1.5 (1.3B)	78.92	78.01	67.56	66.40
phi-2 (2B)	<b>78.98</b>	<b>78.35</b>	<b>67.91</b>	<b>66.67</b>
Qwen2.5 (0.5B)	78.53	77.87	67.70	66.49

Table 7: Ablation of  $d$  on EarthReason Val set.

$d$	#Visual Token	gIoU	$d$	#Visual Token	gIoU
0	1024	68.28	2	64	<b>68.60</b>
1	256	68.47	3	16	68.22

## 6 Conclusion

In this paper, we introduce geospatial pixel reasoning, a new task in remote sensing that requires models to infer segmentation masks from implicit natural language queries by reasoning over spatial context and domain knowledge. To enable research in this direction, we present EarthReason, the first large-scale benchmark dataset that emphasises complex reasoning scenarios. To address the distinct challenges inherent in remote sensing, we propose SegEarth-R1, a language-guided segmentation model that integrates a hierarchical visual encoder, an LLM for instruction parsing and semantic correlation, and a tailored mask generator designed for spatial correlation. Extensive experiments validate SegEarth-R1’s superiority, achieving SOTA performance on both geospatial pixel reasoning and referring segmentation tasks. This work pioneers the fusion of natural language reasoning with pixel-level geospatial analysis, offering transformative potential for applications like environmental monitoring and disaster response.

## References

- [1] Seyed Majid Azimi, Corentin Henry, Lars Sommer, Arne Schumann, and Eleonora Vig. Skyscapes fine-grained semantic understanding of aerial scenes. In *Proceedings of the IEEE/CVF International Conference on Computer Vision*, pages 7393–7403, 2019.
- [2] Lucas Beyer, Andreas Steiner, André Susano Pinto, Alexander Kolesnikov, Xiao Wang, Daniel Salz, Maxim Neumann, Ibrahim Alabdulmohsin, Michael Tschannen, Emanuele Bugliarello, et al. Paligemma: A versatile 3b vlm for transfer. *arXiv preprint arXiv:2407.07726*, 2024.
- [3] Holger Caesar, Jasper Uijlings, and Vittorio Ferrari. Coco-stuff: Thing and stuff classes in context. In *Proceedings of the IEEE conference on computer vision and pattern recognition*, pages 1209–1218, 2018.
- [4] Junbum Cha, Wooyoung Kang, Jonghwan Mun, and Byungseok Roh. Honeybee: Locality-enhanced projector for multimodal llm. In *Proceedings of the IEEE/CVF Conference on Computer Vision and Pattern Recognition*, pages 13817–13827, 2024.
- [5] Bowen Cheng, Ishan Misra, Alexander G Schwing, Alexander Kirillov, and Rohit Girdhar. Masked-attention mask transformer for universal image segmentation. In *Proceedings of the IEEE/CVF conference on computer vision and pattern recognition*, pages 1290–1299, 2022.
- [6] Bowen Cheng, Alex Schwing, and Alexander Kirillov. Per-pixel classification is not all you need for semantic segmentation. *Advances in neural information processing systems*, 34:17864–17875, 2021.
- [7] Wei-Lin Chiang, Zhuohan Li, Ziqing Lin, Ying Sheng, Zhanghao Wu, Hao Zhang, Lianmin Zheng, Siyuan Zhuang, Yonghao Zhuang, Joseph E Gonzalez, et al. Vicuna: An open-source chatbot impressing gpt-4 with 90%\* chatgpt quality. See <https://vicuna.lmsys.org> (accessed 14 April 2023), 2(3):6, 2023.
- [8] Gordon Christie, Neil Fendley, James Wilson, and Ryan Mukherjee. Functional map of the world. In *Proceedings of the IEEE Conference on Computer Vision and Pattern Recognition*, pages 6172–6180, 2018.
- [9] Ilke Demir, Krzysztof Koperski, David Lindenbaum, Guan Pang, Jing Huang, Saikat Basu, Forest Hughes, Devis Tuia, and Ramesh Raskar. Deepglobe 2018: A challenge to parse the earth through satellite images. In *Proceedings of the IEEE conference on computer vision and pattern recognition workshops*, pages 172–181, 2018.
- [10] Henghui Ding, Chang Liu, Suchen Wang, and Xudong Jiang. Vision-language transformer and query generation for referring segmentation. In *Proceedings of the IEEE/CVF International Conference on Computer Vision*, pages 16321–16330, 2021.
- [11] Jian Ding, Nan Xue, Gui-Song Xia, Xiang Bai, Wen Yang, Michael Ying Yang, Serge Belongie, Jiebo Luo, Mihai Datcu, Marcello Pelillo, et al. Object detection in aerial images: A large-scale benchmark and challenges. *IEEE transactions on pattern analysis and machine intelligence*, 44(11):7778–7796, 2021.

- [12] Zhe Dong, Yuzhe Sun, Yanfeng Gu, and Tianzhu Liu. Cross-modal bidirectional interaction model for referring remote sensing image segmentation. *arXiv preprint arXiv:2410.08613*, 2024.
- [13] Mark Everingham, Luc Van Gool, Christopher KI Williams, John Winn, and Andrew Zisserman. The pascal visual object classes (voc) challenge. *International journal of computer vision*, 88:303–338, 2010.
- [14] Rafael C Gonzales and Paul Wintz. *Digital image processing*. Addison-Wesley Longman Publishing Co., Inc., 1987.
- [15] Ritwik Gupta, Richard Hosfelt, Sandra Sajeev, Nirav Patel, Bryce Goodman, Jigar Doshi, Eric Heim, Howie Choset, and Matthew Gaston. xbd: A dataset for assessing building damage from satellite imagery. *arXiv preprint arXiv:1911.09296*, 2019.
- [16] Junwen He, Yifan Wang, Lijun Wang, Huchuan Lu, Jun-Yan He, Jin-Peng Lan, Bin Luo, and Xuansong Xie. Multi-modal instruction tuned llms with fine-grained visual perception. In *Proceedings of the IEEE/CVF conference on computer vision and pattern recognition*, pages 13980–13990, 2024.
- [17] Ngoc-Vuong Ho, Thinh Phan, Meredith Adkins, Chase Rainwater, Jackson Cothren, and Ngan Le. Rssep: Sequence-to-sequence model for simultaneous referring remote sensing segmentation and detection. In *Proceedings of the Asian Conference on Computer Vision*, pages 218–231, 2024.
- [18] Ronghang Hu, Marcus Rohrbach, and Trevor Darrell. Segmentation from natural language expressions. In *Computer Vision—ECCV 2016: 14th European Conference, Amsterdam, The Netherlands, October 11–14, 2016, Proceedings, Part I 14*, pages 108–124. Springer, 2016.
- [19] Yutao Hu, Qixiong Wang, Wenqi Shao, Enze Xie, Zhenguo Li, Jungong Han, and Ping Luo. Beyond one-to-one: Rethinking the referring image segmentation. In *Proceedings of the IEEE/CVF International Conference on Computer Vision*, pages 4067–4077, 2023.
- [20] Zhiwei Hu, Guang Feng, Jiayu Sun, Lihe Zhang, and Huchuan Lu. Bi-directional relationship inferring network for referring image segmentation. In *Proceedings of the IEEE/CVF conference on computer vision and pattern recognition*, pages 4424–4433, 2020.
- [21] Shaofei Huang, Tianrui Hui, Si Liu, Guanbin Li, Yunchao Wei, Jizhong Han, Luoqi Liu, and Bo Li. Referring image segmentation via cross-modal progressive comprehension. In *Proceedings of the IEEE/CVF conference on computer vision and pattern recognition*, pages 10488–10497, 2020.
- [22] Tianrui Hui, Si Liu, Shaofei Huang, Guanbin Li, Sansi Yu, Faxi Zhang, and Jizhong Han. Linguistic structure guided context modeling for referring image segmentation. In *European Conference on Computer Vision*, pages 59–75. Springer, 2020.
- [23] Deyi Ji, Feng Zhao, Hongtao Lu, Mingyuan Tao, and Jieping Ye. Ultra-high resolution segmentation with ultra-rich context: A novel benchmark. In *Proceedings of the IEEE/CVF Conference on Computer Vision and Pattern Recognition*, pages 23621–23630, 2023.
- [24] Lixia Ji, Yunlong Du, Yiping Dang, Wenzhao Gao, and Han Zhang. A survey of methods for addressing the challenges of referring image segmentation. *Neurocomputing*, 583:127599, 2024.
- [25] Alexander Kirillov, Eric Mintun, Nikhila Ravi, Hanzi Mao, Chloe Rolland, Laura Gustafson, Tete Xiao, Spencer Whitehead, Alexander C Berg, Wan-Yen Lo, et al. Segment anything. In *Proceedings of the IEEE/CVF international conference on computer vision*, pages 4015–4026, 2023.
- [26] Xin Lai, Zhuotao Tian, Yukang Chen, Yanwei Li, Yuhui Yuan, Shu Liu, and Jiaya Jia. Lisa: Reasoning segmentation via large language model. In *Proceedings of the IEEE/CVF Conference on Computer Vision and Pattern Recognition*, pages 9579–9589, 2024.

- [27] Mengcheng Lan, Chaofeng Chen, Yue Zhou, Jiaying Xu, Yiping Ke, Xinjiang Wang, Litong Feng, and Wayne Zhang. Text4seg: Reimagining image segmentation as text generation. *arXiv preprint arXiv:2410.09855*, 2024.
- [28] Sen Lei, Xinyu Xiao, Tianlin Zhang, Heng-Chao Li, Zhenwei Shi, and Qing Zhu. Exploring fine-grained image-text alignment for referring remote sensing image segmentation. *IEEE Transactions on Geoscience and Remote Sensing*, 2024.
- [29] Junnan Li, Dongxu Li, Silvio Savarese, and Steven Hoi. Blip-2: Bootstrapping language-image pre-training with frozen image encoders and large language models. In *International conference on machine learning*, pages 19730–19742. PMLR, 2023.
- [30] Kaiyu Li, Ruixun Liu, Xiangyong Cao, Xueru Bai, Feng Zhou, Deyu Meng, and Zhi Wang. Segearth-ov: Towards training-free open-vocabulary segmentation for remote sensing images. *arXiv preprint arXiv:2410.01768*, 2024.
- [31] Ke Li, Gang Wan, Gong Cheng, Liqiu Meng, and Junwei Han. Object detection in optical remote sensing images: A survey and a new benchmark. *ISPRS journal of photogrammetry and remote sensing*, 159:296–307, 2020.
- [32] Ruiyu Li, Kaican Li, Yi-Chun Kuo, Michelle Shu, Xiaojuan Qi, Xiaoyong Shen, and Jiaya Jia. Referring image segmentation via recurrent refinement networks. In *Proceedings of the IEEE Conference on Computer Vision and Pattern Recognition*, pages 5745–5753, 2018.
- [33] Yuanzhi Li, Sébastien Bubeck, Ronen Eldan, Allie Del Giorno, Suriya Gunasekar, and Yin Tat Lee. Textbooks are all you need ii: phi-1.5 technical report. *arXiv preprint arXiv:2309.05463*, 2023.
- [34] Tsung-Yi Lin, Priya Goyal, Ross Girshick, Kaiming He, and Piotr Dollár. Focal loss for dense object detection. In *Proceedings of the IEEE international conference on computer vision*, pages 2980–2988, 2017.
- [35] Chang Liu, Henghui Ding, and Xudong Jiang. Gres: Generalized referring expression segmentation. In *Proceedings of the IEEE/CVF conference on computer vision and pattern recognition*, pages 23592–23601, 2023.
- [36] Chenxi Liu, Zhe Lin, Xiaohui Shen, Jimei Yang, Xin Lu, and Alan Yuille. Recurrent multi-modal interaction for referring image segmentation. In *Proceedings of the IEEE international conference on computer vision*, pages 1271–1280, 2017.
- [37] Haotian Liu, Chunyuan Li, Qingyang Wu, and Yong Jae Lee. Visual instruction tuning. *Advances in neural information processing systems*, 36:34892–34916, 2023.
- [38] Jiang Liu, Hui Ding, Zhaowei Cai, Yuting Zhang, Ravi Kumar Satzoda, Vijay Mahadevan, and R Manmatha. Polyformer: Referring image segmentation as sequential polygon generation. In *Proceedings of the IEEE/CVF Conference on Computer Vision and Pattern Recognition*, pages 18653–18663, 2023.
- [39] Si Liu, Tianrui Hui, Shaofei Huang, Yunchao Wei, Bo Li, and Guanbin Li. Cross-modal progressive comprehension for referring segmentation. *IEEE Transactions on Pattern Analysis and Machine Intelligence*, 44(9):4761–4775, 2021.
- [40] Sihan Liu, Yiwei Ma, Xiaoqing Zhang, Haowei Wang, Jiayi Ji, Xiaoshuai Sun, and Rongrong Ji. Rotated multi-scale interaction network for referring remote sensing image segmentation. In *Proceedings of the IEEE/CVF Conference on Computer Vision and Pattern Recognition*, pages 26658–26668, 2024.
- [41] Sun-Ao Liu, Yiheng Zhang, Zhaofan Qiu, Hongtao Xie, Yongdong Zhang, and Ting Yao. Caris: Context-aware referring image segmentation. In *Proceedings of the 31st ACM International Conference on Multimedia*, pages 779–788, 2023.
- [42] Xu Liu and Zhouhui Lian. Rsunivlm: A unified vision language model for remote sensing via granularity-oriented mixture of experts. *arXiv preprint arXiv:2412.05679*, 2024.

- [43] Ze Liu, Yutong Lin, Yue Cao, Han Hu, Yixuan Wei, Zheng Zhang, Stephen Lin, and Baining Guo. Swin transformer: Hierarchical vision transformer using shifted windows. In *Proceedings of the IEEE/CVF international conference on computer vision*, pages 10012–10022, 2021.
- [44] Yang Long, Gui-Song Xia, Shengyang Li, Wen Yang, Michael Ying Yang, Xiao Xiang Zhu, Liangpei Zhang, and Deren Li. On creating benchmark dataset for aerial image interpretation: Reviews, guidances, and million-aid. *IEEE Journal of selected topics in applied earth observations and remote sensing*, 14:4205–4230, 2021.
- [45] Siqi Lu, Junlin Guo, James R Zimmer-Dauphinee, Jordan M Nieusma, Xiao Wang, Steven A Wernke, Yuankai Huo, et al. Vision foundation models in remote sensing: A survey. *IEEE Geoscience and Remote Sensing Magazine*, 2025.
- [46] Xiaoliang Lu, Binqiang Wang, Xiangtao Zheng, and Xuelong Li. Exploring models and data for remote sensing image caption generation. *IEEE Transactions on Geoscience and Remote Sensing*, 56(4):2183–2195, 2017.
- [47] Edgar Margffoy-Tuay, Juan C Pérez, Emilio Botero, and Pablo Arbeláez. Dynamic multimodal instance segmentation guided by natural language queries. In *Proceedings of the European Conference on Computer Vision (ECCV)*, pages 630–645, 2018.
- [48] Fausto Milletari, Nassir Navab, and Seyed-Ahmad Ahmadi. V-net: Fully convolutional neural networks for volumetric medical image segmentation. In *2016 fourth international conference on 3D vision (3DV)*, pages 565–571. Ieee, 2016.
- [49] Sayan Nag, Koustava Goswami, and Srikrishna Karanam. Safari: Adaptive sequence transformer for weakly supervised referring expression segmentation. In *European Conference on Computer Vision*, pages 485–503. Springer, 2024.
- [50] Ruizhe Ou, Yuan Hu, Fan Zhang, Jiabin Chen, and Yu Liu. Geopix: Multi-modal large language model for pixel-level image understanding in remote sensing. *arXiv preprint arXiv:2501.06828*, 2025.
- [51] Chao Pang, Xingxing Weng, Jiang Wu, Jiayu Li, Yi Liu, Jiabin Sun, Weijia Li, Shuai Wang, Litong Feng, Gui-Song Xia, et al. Vhm: Versatile and honest vision language model for remote sensing image analysis. *arXiv preprint arXiv:2403.20213*, 2024.
- [52] Alec Radford, Jong Wook Kim, Chris Hallacy, Aditya Ramesh, Gabriel Goh, Sandhini Agarwal, Girish Sastry, Amanda Askell, Pamela Mishkin, Jack Clark, et al. Learning transferable visual models from natural language supervision. In *International conference on machine learning*, pages 8748–8763. PmLR, 2021.
- [53] Hanoona Rasheed, Muhammad Maaz, Sahal Shaji, Abdelrahman Shaker, Salman Khan, Hisham Cholakkal, Rao M Anwer, Eric Xing, Ming-Hsuan Yang, and Fahad S Khan. Glamm: Pixel grounding large multimodal model. In *Proceedings of the IEEE/CVF Conference on Computer Vision and Pattern Recognition*, pages 13009–13018, 2024.
- [54] Nikhila Ravi, Valentin Gabeur, Yuan-Ting Hu, Ronghang Hu, Chaitanya Ryali, Tengyu Ma, Haitham Khedr, Roman Rädle, Chloe Rolland, Laura Gustafson, et al. Sam 2: Segment anything in images and videos. *arXiv preprint arXiv:2408.00714*, 2024.
- [55] Zhongwei Ren, Zhicheng Huang, Yunchao Wei, Yao Zhao, Dongmei Fu, Jiashi Feng, and Xiaojie Jin. Pixellm: Pixel reasoning with large multimodal model. In *Proceedings of the IEEE/CVF Conference on Computer Vision and Pattern Recognition*, pages 26374–26383, 2024.
- [56] Esther Rolf, Konstantin Klemmer, Caleb Robinson, and Hannah Kerner. Mission critical—satellite data is a distinct modality in machine learning. *arXiv preprint arXiv:2402.01444*, 2024.
- [57] Akashah Shabbir, Mohammed Zumri, Mohammed Bennamoun, Fahad S Khan, and Salman Khan. Geopixel: Pixel grounding large multimodal model in remote sensing. *arXiv preprint arXiv:2501.13925*, 2025.

- [58] Chao Shang, Zichen Song, Heqian Qiu, Lanxiao Wang, Fanman Meng, and Hongliang Li. Prompt-driven referring image segmentation with instance contrasting. In *Proceedings of the IEEE/CVF Conference on Computer Vision and Pattern Recognition*, pages 4124–4134, 2024.
- [59] Claude E Shannon. A mathematical theory of communication. *The Bell system technical journal*, 27(3):379–423, 1948.
- [60] Hengcan Shi, Hongliang Li, Fanman Meng, and Qingbo Wu. Key-word-aware network for referring expression image segmentation. In *Proceedings of the European Conference on Computer Vision (ECCV)*, pages 38–54, 2018.
- [61] Andreas Steiner, André Susano Pinto, Michael Tschannen, Daniel Keysers, Xiao Wang, Yonatan Bitton, Alexey Gritsenko, Matthias Minderer, Anthony Sherbondy, Shangbang Long, et al. Paligemma 2: A family of versatile vlms for transfer. *arXiv preprint arXiv:2412.03555*, 2024.
- [62] Hugo Touvron, Louis Martin, Kevin Stone, Peter Albert, Amjad Almahairi, Yasmine Babaei, Nikolay Bashlykov, Soumya Batra, Prajjwal Bhargava, Shruti Bhosale, et al. Llama 2: Open foundation and fine-tuned chat models. *arXiv preprint arXiv:2307.09288*, 2023.
- [63] A Vaswani. Attention is all you need. *Advances in Neural Information Processing Systems*, 2017.
- [64] Fengxiang Wang, Hongzhen Wang, Mingshuo Chen, Di Wang, Yulin Wang, Zonghao Guo, Qiang Ma, Long Lan, Wenjing Yang, Jing Zhang, et al. Xlrs-bench: Could your multimodal llms understand extremely large ultra-high-resolution remote sensing imagery? *arXiv preprint arXiv:2503.23771*, 2025.
- [65] Junchi Wang and Lei Ke. Llm-seg: Bridging image segmentation and large language model reasoning. In *Proceedings of the IEEE/CVF Conference on Computer Vision and Pattern Recognition*, pages 1765–1774, 2024.
- [66] Junjue Wang, Zhuo Zheng, Zihang Chen, Ailong Ma, and Yanfei Zhong. Earthvqa: Towards queryable earth via relational reasoning-based remote sensing visual question answering. In *Proceedings of the AAAI Conference on Artificial Intelligence*, volume 38, pages 5481–5489, 2024.
- [67] Junjue Wang, Zhuo Zheng, Ailong Ma, Xiaoyan Lu, and Yanfei Zhong. Loveda: A remote sensing land-cover dataset for domain adaptive semantic segmentation. *arXiv preprint arXiv:2110.08733*, 2021.
- [68] Wenhai Wang, Zhe Chen, Xiaokang Chen, Jiannan Wu, Xizhou Zhu, Gang Zeng, Ping Luo, Tong Lu, Jie Zhou, Yu Qiao, et al. Visionllm: Large language model is also an open-ended decoder for vision-centric tasks. *Advances in Neural Information Processing Systems*, 36:61501–61513, 2023.
- [69] Zhaoqing Wang, Yu Lu, Qiang Li, Xunqiang Tao, Yandong Guo, Mingming Gong, and Tongliang Liu. Cris: Clip-driven referring image segmentation. In *Proceedings of the IEEE/CVF conference on computer vision and pattern recognition*, pages 11686–11695, 2022.
- [70] Zhou Wang, Alan C Bovik, Hamid R Sheikh, and Eero P Simoncelli. Image quality assessment: from error visibility to structural similarity. *IEEE transactions on image processing*, 13(4):600–612, 2004.
- [71] Cong Wei, Yujie Zhong, Haoxian Tan, Yingsen Zeng, Yong Liu, Zheng Zhao, and Yujiu Yang. Instructseg: Unifying instructed visual segmentation with multi-modal large language models. *arXiv preprint arXiv:2412.14006*, 2024.
- [72] Jiannan Wu, Yi Jiang, Peize Sun, Zehuan Yuan, and Ping Luo. Language as queries for referring video object segmentation. In *Proceedings of the IEEE/CVF Conference on Computer Vision and Pattern Recognition*, pages 4974–4984, 2022.
- [73] Jiannan Wu, Muyan Zhong, Sen Xing, Zeqiang Lai, Zhaoyang Liu, Zhe Chen, Wenhai Wang, Xizhou Zhu, Lewei Lu, Tong Lu, et al. Visionllm v2: An end-to-end generalist multimodal large language model for hundreds of vision-language tasks. *Advances in Neural Information Processing Systems*, 37:69925–69975, 2025.

- [74] Jianzong Wu, Xiangtai Li, Xia Li, Henghui Ding, Yunhai Tong, and Dacheng Tao. Towards robust referring image segmentation. *IEEE Transactions on Image Processing*, 2024.
- [75] Zhuofan Xia, Dongchen Han, Yizeng Han, Xuran Pan, Shiji Song, and Gao Huang. Gsva: Generalized segmentation via multimodal large language models. In *Proceedings of the IEEE/CVF Conference on Computer Vision and Pattern Recognition*, pages 3858–3869, 2024.
- [76] Bin Xiao, Haiping Wu, Weijian Xu, Xiyang Dai, Houdong Hu, Yumao Lu, Michael Zeng, Ce Liu, and Lu Yuan. Florence-2: Advancing a unified representation for a variety of vision tasks (2023). URL <https://arxiv.org/abs/2311.06242>, 2023.
- [77] Zunnan Xu, Zhihong Chen, Yong Zhang, Yibing Song, Xiang Wan, and Guanbin Li. Bridging vision and language encoders: Parameter-efficient tuning for referring image segmentation. In *Proceedings of the IEEE/CVF International Conference on Computer Vision*, pages 17503–17512, 2023.
- [78] Cilin Yan, Haochen Wang, Shilin Yan, Xiaolong Jiang, Yao Hu, Guoliang Kang, Weidi Xie, and Efstratios Gavves. Visa: Reasoning video object segmentation via large language models. In *European Conference on Computer Vision*, pages 98–115. Springer, 2024.
- [79] An Yang, Baosong Yang, Beichen Zhang, Binyuan Hui, Bo Zheng, Bowen Yu, Chengyuan Li, Dayiheng Liu, Fei Huang, Haoran Wei, et al. Qwen2. 5 technical report. *arXiv preprint arXiv:2412.15115*, 2024.
- [80] Senqiao Yang, Tianyuan Qu, Xin Lai, Zhuotao Tian, Bohao Peng, Shu Liu, and Jiaya Jia. Lisa++: An improved baseline for reasoning segmentation with large language model. *arXiv preprint arXiv:2312.17240*, 2023.
- [81] Zhao Yang, Jiaqi Wang, Yansong Tang, Kai Chen, Hengshuang Zhao, and Philip HS Torr. Lavt: Language-aware vision transformer for referring image segmentation. In *Proceedings of the IEEE/CVF Conference on Computer Vision and Pattern Recognition*, pages 18155–18165, 2022.
- [82] Linli Yao, Lei Li, Shuhuai Ren, Lean Wang, Yuanxin Liu, Xu Sun, and Lu Hou. Deco: Decoupling token compression from semantic abstraction in multimodal large language models. *arXiv preprint arXiv:2405.20985*, 2024.
- [83] Linwei Ye, Mrigank Rochan, Zhi Liu, and Yang Wang. Cross-modal self-attention network for referring image segmentation. In *Proceedings of the IEEE/CVF conference on computer vision and pattern recognition*, pages 10502–10511, 2019.
- [84] Haobo Yuan, Xiangtai Li, Tao Zhang, Zilong Huang, Shilin Xu, Shunping Ji, Yunhai Tong, Lu Qi, Jiashi Feng, and Ming-Hsuan Yang. Sa2va: Marrying sam2 with llava for dense grounded understanding of images and videos. *arXiv preprint arXiv:2501.04001*, 2025.
- [85] Zhenghang Yuan, Lichao Mou, Yuansheng Hua, and Xiao Xiang Zhu. Rrsis: Referring remote sensing image segmentation. *IEEE Transactions on Geoscience and Remote Sensing*, 2024.
- [86] Yang Zhan, Zhitong Xiong, and Yuan Yuan. Rsvg: Exploring data and models for visual grounding on remote sensing data. *IEEE Transactions on Geoscience and Remote Sensing*, 61:1–13, 2023.
- [87] Ao Zhang, Yuan Yao, Wei Ji, Zhiyuan Liu, and Tat-Seng Chua. Next-chat: An lmm for chat, detection and segmentation. *arXiv preprint arXiv:2311.04498*, 2023.
- [88] Ao Zhang, Yuan Yao, Wei Ji, Zhiyuan Liu, and Tat-Seng Chua. Next-chat: An lmm for chat, detection and segmentation. In *International Conference on Machine Learning*, pages 60116–60133. PMLR, 2024.
- [89] Tao Zhang, Xiangtai Li, Hao Fei, Haobo Yuan, Shengqiong Wu, Shunping Ji, Chen Change Loy, and Shuicheng Yan. Omg-llava: Bridging image-level, object-level, pixel-level reasoning and understanding. *Advances in Neural Information Processing Systems*, 37:71737–71767, 2025.
- [90] Yichi Zhang, Ziqiao Ma, Xiaofeng Gao, Suhaila Shakiah, Qiaozhi Gao, and Joyce Chai. Groundhog: Grounding large language models to holistic segmentation. In *Proceedings of the IEEE/CVF conference on computer vision and pattern recognition*, pages 14227–14238, 2024.

- [91] Yuxuan Zhang, Tianheng Cheng, Rui Hu, Lei Liu, Heng Liu, Longjin Ran, Xiaoxin Chen, Wenyu Liu, and Xinggang Wang. Evf-sam: Early vision-language fusion for text-prompted segment anything model. *arXiv preprint arXiv:2406.20076*, 2024.
- [92] Zheng Zhang, Yeyao Ma, Enming Zhang, and Xiang Bai. Psalm: Pixelwise segmentation with large multi-modal model. In *European Conference on Computer Vision*, pages 74–91. Springer, 2024.
- [93] Bolei Zhou, Hang Zhao, Xavier Puig, Sanja Fidler, Adela Barriuso, and Antonio Torralba. Scene parsing through ade20k dataset. In *Proceedings of the IEEE conference on computer vision and pattern recognition*, pages 633–641, 2017.
- [94] Li Zhou, Xu Yuan, Zenghui Sun, Zikun Zhou, and Jingsong Lan. Instruction-guided multi-granularity segmentation and captioning with large multimodal model. *arXiv preprint arXiv:2409.13407*, 2024.
- [95] Yue Zhou, Mengcheng Lan, Xiang Li, Yiping Ke, Xue Jiang, Litong Feng, and Wayne Zhang. Geoground: A unified large vision-language model. for remote sensing visual grounding. *arXiv preprint arXiv:2411.11904*, 2024.

## A Data

### A.1 Annotation of EarthReason

Each sample of the EarthReason benchmark consists of an image, a corresponding mask, and six reasoning queries along with their respective answers. Given that our metadata is derived from classification datasets, we employed GPT-4o and GPT-3.5 to generate textual annotations, and invited multiple remote sensing and vision experts to provide accurate and reliable mask annotations. Overall, our annotation process consists of the following three steps:

- Step-1: To fully leverage the powerful multimodal capabilities and extensive geographic knowledge of GPT-4o, we carefully design the prompt, which is then provided alongside images and their corresponding category labels to generate a reasoning question–answer pair. The prompt is illustrated in Figure 6.
- Step-2: To avoid homogeneous question–answer formats under a single prompt, we further employ the textual capabilities of GPT-3.5 to expand each generated question into six variations and each answer into three alternatives. The prompt used for this expansion is shown in Figure 7.
- Step-3: Unlike previous methods that rely on semi-automatic mask annotation based on off-the-shelf bounding boxes or masks, we invite multiple remote sensing vision experts to perform accurate and efficient mask annotation guided by the generated questions. To further improve annotation efficiency, we incorporate SAM-H as an auxiliary tool for some simple targets. Subsequently, we perform cross-validation of the annotation results and re-annotate the samples that do not meet the quality standards. As shown in Figure 8, (a), (b), and (c), derived from the RRSIS-D dataset, illustrate the masks of semi-automatic annotation based on bounding boxes. (a) and (c) exhibit noticeable annotation errors, while in (b), the query does not align with the annotation. (d), (e), and (f) illustrate our high-quality manual annotations.

**Prompt:** You are an expert in geographic remote sensing imagery. Please fully analyze the geographical landscape and cultural features in remote sensing images. Generate an implicit reasoning questions based on given object categories. Please use your imagination and feel free to change the sentence structure or add a situation description. Just give the implicit reasoning questions that meet the requirements. The descriptions must refer to the natural landscapes and cultural landscapes shown in remote sensing images. The output implicit reasoning questions need to meet the following requirements:

- (1) Please imagine the scene and output an implicit reasoning question to describe the attributes or functions of the given object. The output question must have a certain degree of reasoning difficulty and be helpful to humans.
- (2) Do not explicitly write the name or description of the target object in the original text. Questions should be asked in the form of asking where, which infrastructure, how to do a certain activity, which location, what object.
- (3) The output cannot be redundant. Just give one question and its answer that you think has the highest confidence. The question should be at least 18 words. The answer requires giving the name of the given object and then explaining why the answer is this, about 20 words.
- (4) Do not output any redundant information except the question and the answer, and separate them with line break.

The given object category is <ground track field>. <image>



⌘ ... ..

**Question:** If an earthquake were to occur, what is the most secure area to assemble numerous individuals that also facilitates emergency service access?

**Answer:** The [ground track field](#) stands out as the most secure location, thanks to its vast open area that minimizes the chance of hazards, as well as its close accessibility to primary roads for swift emergency response.

Figure 6: The illustration of the prompt construction process for generating question-answer pairs for geospatial pixel reasoning.

### A.2 EarthReason Statistics

The EarthReason benchmark comprises 28 categories, and the number of samples in each category is shown in Figure 9 (a). It can be observed that the distribution of the 28 categories is relatively balanced. Figure 9 (b), (c), and (d) illustrate the category distributions in the training, validation, and test sets, respectively. To evaluate the model’s generalization capability, we specifically excluded four categories—“basketball court”, “island”, “lake”, and “stadium”—from the training set. Moreover, we introduced 119 empty target samples to mitigate potential hallucinations of the model.

**Prompt:** Imagine you are a remote sensing expert with extensive knowledge in geography. I will give you a question or description related to remote sensing, and you will expand it into 6 related questions or topics. The given question is “If an earthquake were to occur, what is the most secure area to assemble numerous individuals that also facilitates emergency service access?”

⌘ ... ..

**Response:** 1. In case of an earthquake, where can individuals find a clear and accessible area nearby to assemble safely? 2. During an earthquake, what spacious and unobstructed area close by would provide the safest environment for all of us to meet? 3. Should an earthquake happen, where in the vicinity can people find an open area to come together safely and securely? 4. In the scenario of an earthquake, where can residents find a secure area with open space and accessible paths for evacuation? 5. In an earthquake situation, which nearby area featuring open space and clear pathways would be the safest choice for resident evacuation? 6. If an earthquake occurs, which types of infrastructure are anticipated to function as dependable gathering spots with adequate open areas?

**Prompt:** Imagine you are a remote sensing expert with extensive knowledge in geography. I will give you a question or description related to remote sensing, and you will expand it into 3 related questions or topics. The given description is “The ground track field stands out as the most secure location, thanks to its vast open area that minimizes the chance of hazards, as well as its close accessibility to primary roads for swift emergency response.”

⌘ ... ..

**Response:** 1. With minimal obstructions and easy access to main roads, the ground track field offers both safety and convenience, positioning it as the most reliable site in terms of hazard prevention and emergency preparedness. 2. The expansive open space of the track field provides a secure environment, greatly minimizing the chance of falling objects. This makes it an ideal refuge from any potential dangers. 3. With its generous outdoor space devoid of any encroaching structures, the ground track field emerges as the premier choice, ensuring an environment where safety is prioritized.

Figure 7: The illustration of the prompt construction process for expand question-answer pairs.

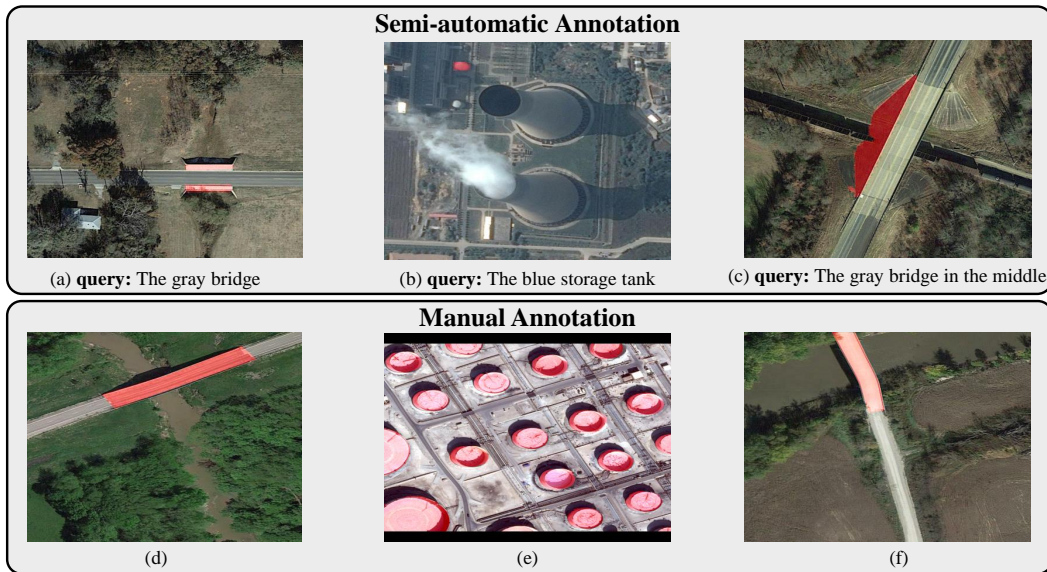


Figure 8: Comparison of annotation quality. (a), (b) and (c) are from RRSIS-D dataset, (d), (e) and (f) are from our EarthReason dataset.

## B Additional Implementation Details

### B.1 Details of Training Hyper-parameters

Table 8 presents the hyper-parameter settings used during the training of our model. For training on the referring segmentation datasets, we employ only focal loss and dice loss to supervise mask generation. In contrast, for training on geospatial pixel reasoning task, we additionally incorporate the cross-entropy loss from the large language model to supervise text answer generation.

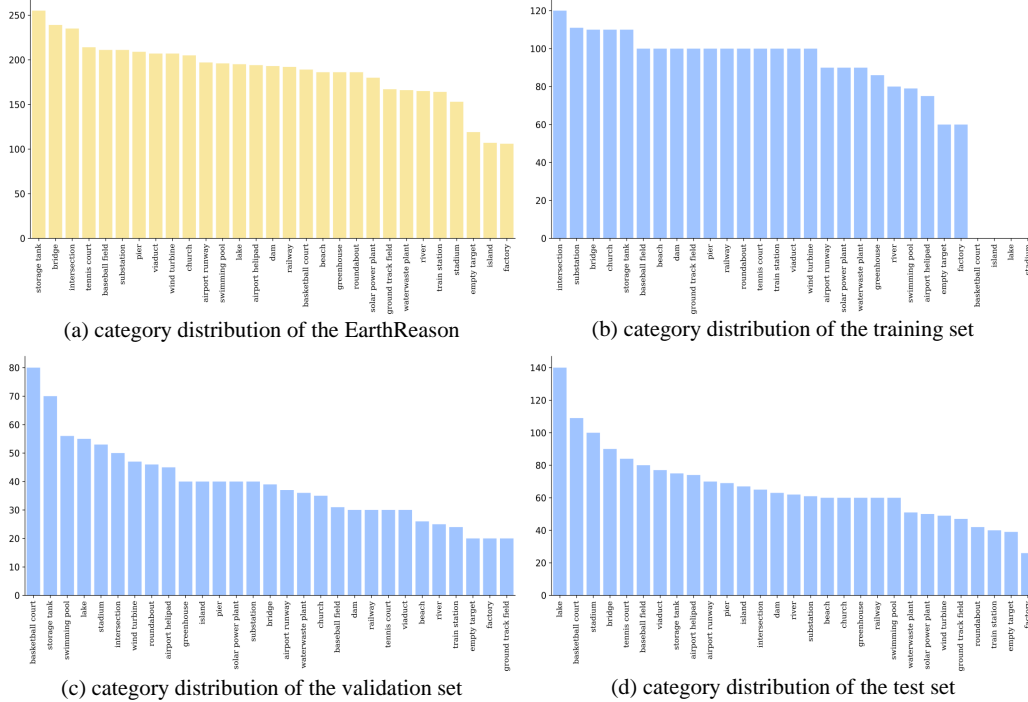


Figure 9: The category distribution of EarthReason.

Table 8: The hyper-parameters for model training.

Parameters	Value
Optimizer	AdamW
Learning Rate	$1 \times 10^{-4}$
Batch Size	16
Number of Iteration	7,610 / 5,400 / 2,220
Learning Rate Schedule	Cosine Decay
Weight Decay	0.0
Warmup Ratio	0.03
$\beta_1$	0.9
$\beta_2$	0.999
Image Size	$1024 \times 1024$
Image Processing	Resize long edge to 1024 and padding short edge to 1024.

## C Examples

### C.1 More Qualitative Results on EarthReason

Figure 10 presents a comparison between SegEarth-R1 and other models on the EarthReason dataset. It can be observed that our model demonstrates a better understanding of long reasoning instructions and produces more accurate mask generation.

### C.2 More Qualitative Results on RRSIS-D

Figure 11 presents a comparison between SegEarth-R1 and PSALM on the RRSIS-D dataset. Our model demonstrates a better understanding of direct geographical attributes such as location, color, and size compared to PSALM. This improvement is attributed to the removal of indirect mask

prediction using mask tokens, allowing semantic information (description embeddings) to directly interact with image features to generate masks.



Figure 10: Comparison with other models on EarthReason.

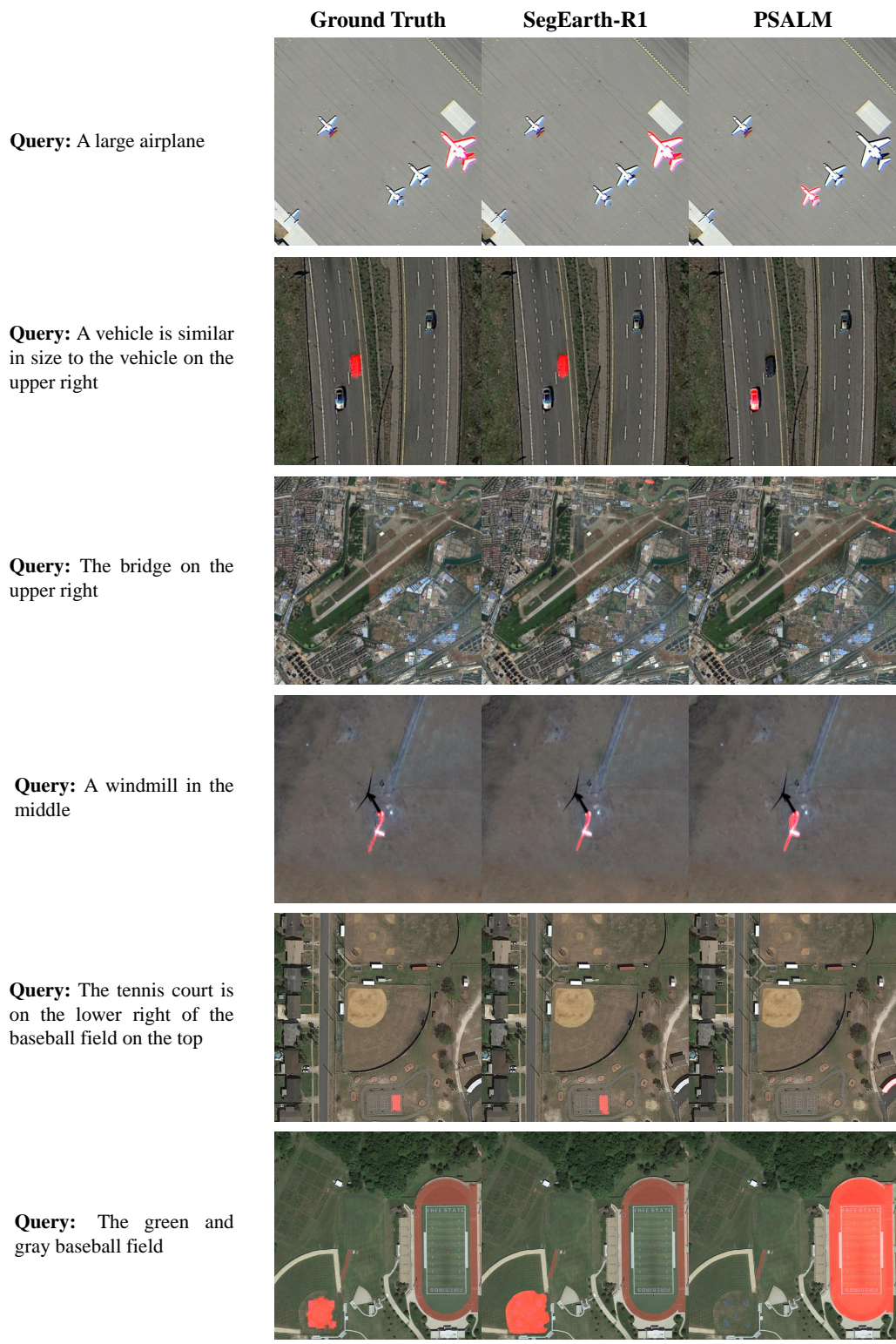


Figure 11: Comparison with PSALM on RRSIS-D.